Polymer Bulletin (2023) 80:6749–6775
https://doi.org/10.1007/s00289-022-04375-z

ORIGINAL PAPER

Mechanical, antibacterial, and non-cytotoxic performance of polypropylene nanocomposites reinforced with $sTiO_2$ deposited with AgNPs mediated by quercetin biomolecule

M. G. Peña-Juarez[1] · L. O. Sanchez-Vargas[2] · L. A. Flores-Gonzalez[3] · A. Almendarez-Camarillo[4] · E. J. Gutierrez-Castañeda[5] · J. Navarrete-Damian[6] · E. Pérez[7] · J. A. Gonzalez-Calderon[8]

Received: 14 April 2022 / Revised: 12 June 2022 / Accepted: 7 July 2022 /
Published online: 26 July 2022
© The Author(s), under exclusive licence to Springer-Verlag GmbH Germany, part of Springer Nature 2022

Abstract

In this work, the mechanical, antibacterial, and non-cytotoxic performance of isotactic polypropylene (iPP) nanocomposites was evaluated when silanized TiO_2 ($sTiO_2$) nanoparticles deposited with AgNPs were used as filler. The synthesis and deposition on $sTiO_2$ were carried out using the quercetin biomolecule as reducing and stabilizing agents, as green approach. One-step and two-step methods were compared, and two qualities of quercetin were used: reactive grade (99% purity) and dietary supplement (20% purity). Both methods were characterized by UV, TEM, EDX, XRD, and Z potential. For nanocomposites, iPP was prepared with $sTiO_2$-AgNPs at

✉ J. A. Gonzalez-Calderon
amir@ifisica.uaslp.mx

1 Doctorado Institucional en Ingeniería y Ciencia de Materiales, Universidad Autónoma de San Luis Potosí, Sierra Leona No. 550 Col. Lomas 2da. Sección, 78210 San Luis Potosí, SLP, México

2 Laboratorio de Microbiología. Facultad de Estomatología, Universidad Autónoma de San Luis Potosí, Zona Universitaria, Av. Manuel Nava #64, 78290 San Luis Potosí, SLP, México

3 Tecnológico Nacional de México/Instituto Tecnológico de Orizaba, Oriente 9 No. 852 Emiliano Zapata, Orizaba, Veracruz, México

4 Departamento de Ingeniería Química, Tecnológico Nacional de México en Celaya, Av. Tecnológico y Antonio García Cubas S/N., 38010 Celaya, Guanajuato, México

5 Cátedras CONACYT-Instituto de Metalurgia, Universidad Autónoma de San Luis Potosí, Av. Sierra Leona 550, Lomas 2da Sección, 78210 San Luis Potosí, SLP, México

6 Tecnológico Nacional de México/CRODE Celaya, Diego Arenas Guzmán 901, Fracc. Zona de Oro 1, 38020 Guanajuato, México

7 Instituto de Física, Universidad Autónoma de San Luis Potosí, Álvaro Obregón 64, 78000 San Luis Potosí, SLP, México

8 Cátedras CONACYT-Instituto de Física, Universidad Autónoma de San Luis Potosí, Av. Manuel Nava #6 Zona Universitaria, 78290 San Luis Potosí, SLP, México

two ratios, 0.5 and 1% w/w, to evaluate whether the nanoparticles can confer antimicrobial activity and improve their mechanical properties. The antibacterial activity was studied against *Escherichia coli* and S*taphylococcus aureus*, and the mechanical properties were evaluated by dynamic mechanical analysis. The best nanomaterial was prepared by the one-step method using quercetin dietary supplement, with the highest silver content (7.0%) and the most significant antibacterial activity, with an improvement of 40%. As for the nanocomposites, those prepared at 0.05% w/w with the one-step method presented the best dynamic mechanical properties, because the fillers were well dispersed and significantly improved the integration and stress dissipation, thus enhancing the antimicrobial capacity. Finally, cytotoxic activity evaluation found that nanocomposites of iPP with sTiO_2-AgNPs are non-toxic, unlike single AgNPs. These findings open the possibility of using these nanocomposites with high antimicrobial power and without cytotoxic effects at industrial and commercial level in medicine, food, environment, among others.

Graphical abstract

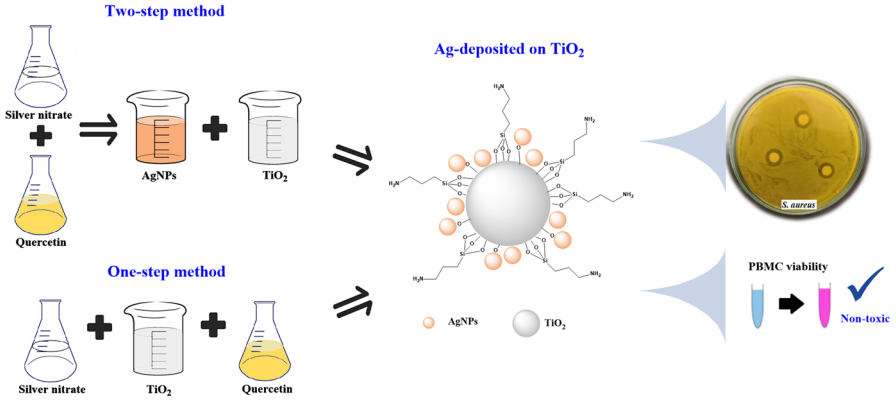

Keywords Silver nanoparticles (AgNPs) · Titanium dioxide nanoparticles · Polypropylene · Antibacterial study · Non-cytotoxicity activity

Introduction

The potential uses for polymers seem to be endless, as they are found in virtually every aspect of daily life. Among the most widely used polymers in the world today is polypropylene (PP) [1]. Polypropylene is a saturated polyolefin containing only carbons and hydrogens in its semi-crystalline structure. It is one of the most widely used polymers in various industries, as it is very hard, opaque and with high heat resistance and it softens at a temperature above 150 ºC. Its main advantage is that it has low production costs [2, 3]. The mechanical properties of polypropylene are highly dependent on its molecular structure, crystallinity and level of orientation [3]. Isotactic polypropylene (iPP) is one of the greatest industrial interest due to its

better mechanical properties, derived from its crystallinity due to its more stereoregular structure. In addition to the advantages mentioned above, PP continues to be improved using fillers or reinforcements that improve its mechanical properties. The most used fillers can range from dicarboxylic salts to various metal oxides that can also be functionalized [4–6], which could also provide other characteristics such as better integration of the fillers within the matrix, or even antimicrobial properties [7, 8].

Nanoparticle-filled polymeric nanocomposites have received great attention in recent years due to their improved mechanical, chemical, optical and electrical properties [9, 10]. For nanocomposites to be successful, the fillers must be integrated in such a way that the adhesion between the particle and the polymeric matrix is optimal. For this reason, the choice of filler is essential in order to achieve improved properties. The main problem on the study of nanocomposites is the tendency of the particles to agglomerate, resulting in poor mechanical and optical properties. One of the options to overcome this problem and to achieve an optimal improvement of the properties is the use of dispersants and coupling agents [7, 8] by functionalizing the surface of the nanoparticles. Silanization is a great option as it modifies the surface of metal oxides, changing their attractive interaction and helping to reduce the problem of agglomeration [11–14].

Bacterial resistance is currently causing many problems in areas such as medicine and food, as pathogenic bacteria that cause infections and trigger diseases are embedded in polymers as reservoirs and are often the most significant source of contagion. To solve this problem, composites or surfaces can be prepared with biocidal materials, such as nanoparticles, to inhibit or eliminate bacteria. Therefore, the importance of developing antimicrobial contact surfaces as a sanitary tool in the control the spread of these types of diseases. To open a broad perspective of PP to more industrial applications, researchers have worked to incorporate fillers, which allow improving the antimicrobial and mechanical properties of the film.

Pathogenic bacteria cause infections in humans, triggering diseases causing a high impact on public health and immense economic losses [15]. The main ways that bacteria can infect are through (1) hosts, any animal or plant in which a bacterium lives, and (2) reservoirs, any site, animal, or plant where the bacteria can survive and multiply until its transfer to a host [16]. Nonliving reservoirs are often the most significant source of contagion since every object, device, food, air, soil, and water can transmit infections [17]. For example, feces may contaminate raw fruits and vegetables in soil, spores on air, or bacteria in the water, becoming reservoirs for *Escherichia coli* (*E. coli*) [18, 19], while S*taphylococcus aureus (S. aureus)*, a major bacterial human pathogen, is typically found on human skin, mucus membranes, nose, armpit, groin, and other areas, which can cause the infection of tissues, lungs, abdomen, heart valves, etc. [20, 21]. Although the action against bacteria is relatively simple, the concern about bacterial infections has rapidly grown due to two main facts: the resistance to antimicrobials and the lack of antibacterial surfaces that facilitate the spread of diseases by transmission through contaminated objects.

Therefore, it is urgent to develop antibacterial materials against pathogenic bacteria [17]. Recently, silver nanoparticles (AgNPs) have proven to be a great alternative as effective antibacterial agents. Several works [22, 23] have proposed that they

possess more than one action mechanism against bacteria; for example, AgNPs may bind strongly to the bacterial membrane and incorporate them into the cell, causing leakage of intracellular substances and penetrating the bacteria [22–24]. However, in recent years AgNPs have raised alarms about their potential hazards to the health, safety, and environment [25]. In addition, from in vitro cell culture tests, it has been reported that, depending on dose, shape, size (< 10 nm), surface charge, and condition, these nanoparticles have toxic effects on various human cell lines, including human peripheral blood mononuclear cells [26, 27]. Therefore, despite their antibacterial action, they have the inherent counterpart of inducing cytotoxicity effects in mammalian cells [28].

In addition, working with nanoparticles can bring challenges, such as spontaneous agglomeration and instability in the air, water, or sunlight, limiting their antibacterial performance [29, 30]. One of the most suitable alternatives is to deposit the AgNPs on the surface of metallic oxides such as titanium dioxide (TiO_2). Thus, materials deposited with AgNPs can be well-dispersed without aggregation [22–24, 29–33] and lower toxicity [26–28]. TiO_2 has arisen as an excellent material thanks to being non-toxic and an exceptional degradant of organic pollutants [24, 29, 34]. In addition, it is a chemically stable amphoteric oxide that is used as a photocatalyst to degrade organic molecules [18–21] and prevents bacterial contamination and infection [35, 36]. There are several examples of Ag-deposition on titanium dioxide nanoparticles; most of them are performed in two steps: first AgNPs are obtained and then deposited on silanized $sTiO_2$. Although these methods have shown promising results, they need a long time for the reaction process and lead to agglomeration of the particles limiting the product's quality and industrial applicability [37].

Lately, the synthesis of nanoparticles using biomolecules has increased for their simple, ecological, and non-toxic nature [38]. These eco-friendly processes, often called green synthesis, present a great option thanks to the possibility of controlling the size, shape, and properties of nanoparticles [39]. For example, to obtain AgNPs by reducing silver ions provided by a precursor salt, polyphenolic compounds (PPCs) can reduce Ag^+ ions because hydroxyl (-OH) groups in their aromatic benzene rings scavenge free radicals or chelate free metal ions. Quercetin is the most abundant PPC found in many plants and foods, such as berries, purple onion grapes, garlic, and others.

Using green syntheses is the main advantage of avoiding toxic chemical substances that cause inefficient processes and hazardous waste [40, 41]. Jain and Mehata and Saha et al. [39, 42] have recently used this natural PPC to synthesize silver nanoparticles (AgNPs) by reducing metal ions. In these mechanisms, the primary molecule in the natural extracts is quercetin. It is used as a protective and reducing agent to induce the formation and stabilization of AgNPs. However, most of the work has been limited to plant extracts, roots, and leaves. Still, there are several drawbacks, such as the variability of raw materials and the poor control of flavonoid content that can be affected by maturity, moisture, size, and poor stability of these perishable materials.

In this work, it was evaluated whether antimicrobial properties could be conferred to iPP by using silanized titanium dioxide ($sTiO_2$) fillers deposited with AgNPs, and how the immersion of these fillers affects the dynamic mechanical properties

of nanocomposites. The obtaining and deposition of AgNPs on $sTiO_2$ were evaluated by two routes: A one-step method, "in situ", was proposed to evaluate whether it is possible to obtain comparable or better results than the two-step method that first performs the reduction and formation of AgNPs and then the deposition on the surface of $sTiO_2$. Both methods were carried out through a green synthesis using quercetin as a reducing agent. The quality of the quercetin was evaluated using reactive grade (99% purity) and dietary supplement quality (20% purity). Therefore, four $sTiO_2$-Ag nanosystems were obtained and analyzed to know which conditions are more favorable to get more silver on the surface and have more antibacterial activity against pathogenic bacteria. On the other hand, the proposal to confer this property to PP was evaluated by microbiological tests on the nanocomposites by drop test and to rule out that they were cytotoxic by performing the resazurin test. Finally, it was evaluated how each different nanosystem was integrated into the polymeric matrix by means of a dynamic mechanical analysis.

Materials and methods

Materials

Reactive grade quercetin (99% purity) was obtained from Sigma-Aldrich. Quercetin dietary supplement (20% purity) was obtained from the "Essential Nutrition" brand, containing quercetin and microcrystalline cellulose. Rutile titanium dioxide (TiO_2) particles (average diameter 350 nm) were obtained from DuPont Mexico (R-104). 3-Aminopropyltriethoxysilane (APTES, 97% purity) was supplied by Sigma-Aldrich (Mexico). Silver nitrate ($AgNO_3$, 99.0%) was provided by Sigma-Aldrich (Mexico).

Obtaining and characterization of AgNPs nanoparticles using quercetin

First, a 1 mM quercetin solution was prepared by dissolving the quercetin in a solution of ethyl alcohol and distilled water (50% v/v) at pH 11. Next, the concentration of this quercetin solution (1 mM) was prepared considering the actual amount of quercetin (99% in the reactive grade and 20%) in the supplement). Next, $AgNO_3$ was dissolved in distilled water to obtain a 2 mM silver nitrate solution. Next, 0.75 mL of the quercetin solution was added to 10 mL of the $AgNO_3$ solution, and it was stirred at 500 rpm for 2 h.

Obtaining of the AgNPs was confirmed by Ultraviolet–visible (UV–Vis) spectroscopy using a Perkin Elmer Model Lambda 35, recording wavelength from 200 to 800 nm at a wavelength. The surface morphology and size of the AgNPs were analyzed using a transmission electron microscope (TEM) using JEOL equipment (model JEM 1230 microscope) with a resolution of 0.4 nm and an acceleration voltage of 100 kV. The particle size distribution was determined by processing TEM images with ImageJ software.

Functionalization of titanium dioxide nanoparticles with APTES

Titanium dioxide was superficially modified with APTES in a 5:1 proportion. Titanium dioxide was mixed with ethanol and stirred and sonicated until completing 2.5 h, as reported in previous work [7]. Subsequently, APTES was added and stirred overnight. The obtained product was washed with water twice and with methanol five times to remove the unreacted agent. Finally, the product was dried in an oven at 80 °C for 6 h. The dried powder was stored and labeled as $sTiO_2$.

Preparation of Ag-deposited $sTiO_2$ nanoparticles

a) Two-step method (M1)

First, a 1-mM solution was prepared by mixing 0.03 g of quercetin with 100 ml of a solution of ethyl alcohol and distilled water (50% v/v); then, pH was adjusted to 11 with NaOH (0.5 M), while 0.034 g of $AgNO_3$ was dissolved in 1000 ml of distilled water to obtain a 2-mM silver nitrate solution. Finally, 1 ml of the quercetin solution was added to 10 mL of the $AgNO_3$ solution and vigorously stirred for 2 h, and then, it was kept undisturbed for 24 h to complete the AgNPs formation.

Second, 10 g of $sTiO_2$ was mixed with 250 ml of water and sonicated for 5 min at 60 Hz in an ultrasonic bath. While stirring, the previous AgNPs colloidal solution (250 mL) was added, and the mixture was stirred for 2 h to complete the deposition. Then, drying was carried out in an oven at 80 °C overnight. The dried powder was stored and labeled as M1R1.

The above procedures were repeated for the quercetin dietary supplement. In addition, the obtained powder was labeled as M1S2.

b) One-step method (M2)

Ten grams of $sTiO_2$ was mixed with 250 ml of water and sonicated for 5 min at 60 Hz in an ultrasonic bath, while 0.085 g of $AgNO_3$ was dissolved in 250 ml distilled water to obtain a 2-mM silver nitrate solution and added to the $sTiO_2$ solution. Finally, a 1-mM quercetin solution was prepared in a solution of ethyl alcohol and distilled water (50% v/v) and adjusted to a pH of 11 with NaOH (0.5 M), and 25 mL of this solution added to the main vessel. The reaction was stirred for 24 h to complete the AgNPs formation and deposition "in situ". Then, drying was carried out in an oven at 80 °C overnight. The dried powder was stored and labeled as M2R1.

The previous procedure was repeated for quercetin dietary supplement. The obtained powder was labeled as M2S2.

Characterization of titanium dioxide nanoparticles silanized with APTES

Pristine TiO_2 and silanized TiO_2 ($sTiO_2$) were characterized by Fourier transform infrared spectrometry (FTIR), using a Perkin model spectrum 100 spectrometer

to confirm the successful demonstration of chemical modification by bonding of APTES to the surface of titanium dioxide. Each spectrum was recorded between 4000 and 1000 cm^{-1} with 80 scans per sample.

Characterization of Ag deposited on $sTiO_2$ nanoparticles

Transmission electron microscopy (sTEM) analysis was performed to confirm the Ag deposition. The four samples, M1R1, M1S2, M2R1, and M2S2, were dispersed in an aqueous medium, making serial dilutions until achieving the optimum particle concentration. Finally, a drop was placed on a copper grid and observed in JEOL equipment (model JEM 1230 microscope) with a resolution of 0.4 nm and an acceleration voltage of 100 kV.

The X-ray diffraction (XRD) measurements for the four samples were used to investigate the crystalline structure of the Ag deposited on $sTiO_2$ by using a Bruker Model D8 ADVANCE diffractometer with Lynx Eye detector and copper tube (wavelength 1.5406A). The samples (2θ) were scanned at 20–80° with a 0.02° increment.

The hydrodynamic diameter and the surface charge (Zeta potential) were characterized by a Delsa Nano C Particle Analyzer (Beckman Coulter). For particle size, the nanoparticles were suspended in water. While for Z potential, colloidal solutions were prepared and scanned at different pHs to monitor the behavior of nanoparticles.

The colloidal stability analysis of the systems was performed through a piece of equipment designed by our research group, consisting of a light-emitting unit and a receiver that translates the light intensity. This equipment scans along with a quartz cell where the suspension is located. The suspensions were studied at 0, 4, 24, 48, and 72 h.

Antimicrobial activity of Ag deposited on $sTiO_2$ nanoparticles by disk diffusion method

The four systems were tested against pathogenic bacteria to evaluate their antimicrobial effects. The susceptibility of Gram-positive bacteria (*Staphylococcus aureus* ATCC-47077) and Gram-negative bacteria (*Escherichia coli* ATCC-25922) was tested by the disk diffusion method [43]. First, the disks were placed in vials, soaked with each freshly prepared system, and left to impregnate. Next, the microbial strains of bacteria, *E. coli* and *S. aureus*, were inoculated into the nutrient broth and kept overnight for incubation in a furnace. The turbidity of broth cultures was compared with 0.5 McFarland solutions, corresponding to $1–2 \times 10^8$ colony-forming units (CFU ml^{-1}). The solid growth medium used for *S. aureus* and *E. coli* was mannitol agar and coliform chromogenic agar, respectively. Next, Petri dishes were inoculated using a sterile swab with the microorganisms, rotating the box 60° for each striatum application. Finally, the disks previously impregnated were placed on each dish and incubated in a furnace at 37 °C for 24 h. Finally, the zones of inhibition (halo) o were measured under an extraction hood. The assays were performed in triplicate, and mean values of zone diameter were taken using the ImageJ software.

Preparation of the iPP nanocomposites

Two ratios of $sTiO_2$ were used as filler in the iPP matrix. The percentages in weight tested to study their antibacterial activity conferred by the nanoparticles were 0.5% w/w and 1% w/w. The nanocomposites were prepared by extrusion in a twin-screw extruder with a heating profile in the feed section at 190 °C, heating section at 240 °C and die at 190 °C was used. All nanocomposites were extruded three times to improve the nanoparticles dispersion in the polymer matrix.

Antibacterial analysis of iPP nanocomposites by the drop-test method

iPP nanocomposites were tested against *S. aureus* and *E. coli* using the antibacterial drop-test method [36] with some modifications. Each nanocomposite was immersed in a test tube with nutrient broth inoculated with the respective bacteria. Moreover, a culture of the microorganism was grown without any treatment as a control. Then, the tubes were incubated for 24 h and then measured in a spectrophotometer. The optical absorptions [A] were recorded, and the inhibition rate (%) is calculated as follows:

$$\text{Inhibition rate}(\%) = \frac{[A]_i - [A]_c}{[A]_i} \times 100 \tag{1}$$

where $[A]_i$ is the optical absorption of the control, and $[A]_c$ is the absorption of each nanocomposite.

Dynamic mechanical analysis

A dynamic mechanical analyzer (DMA-8000 PerkinElmer) was used to determine the viscoelastic properties for the iPP nanocomposites. The configuration was set dual cantilever with a displacement amplitude of 0.05 mm under constant strain and a frequency of 1 Hz. The evolution of the storage modulus, loss modulus, and Tan δ as a function of the temperature (between −20 and 120 °C with a ramp of 3 °C/min) were analyzed.

Evaluation of cell viability of Ag deposited on $sTiO_2$ nanoparticles by Resazurin method

The resazurin method assessed cell viability by seeding peripheral blood mononuclear cells (PBMC) (Sigma-Aldrich). The PBMC was isolated by Ficoll-Histopaque gradient (Histopaque1077, Sigma-Aldrich). Subsequently, the different nanoparticles were exposed to PBMC in different concentrations in a supplemented RPMI-1640 medium (50 U/ml of penicillin and 50 mg/ml) streptomycin) for 24 h. Cell viability of the nanocomposites was also evaluated by exposing mononuclear cells to different concentrations of solutions resulting from the immersion in deionized water and subsequent sonication for 30 min at 60 Hz in an ultrasonic bath of each

nanocomposite. Cell viability was evaluated by the percentage of mitochondrial activity concerning the negative control. The rate of mitochondrial activity was assessed using fluorescence reading at a wavelength of λ = 560 nm of excitation and λ = 590 nm of emission. Cell viability of all dosing treatments was determined in triplicate using the following equation:

$$\text{Cell viability } (\%) = \frac{F_S}{F_C} \times 100\% \tag{2}$$

where F_s is the fluorescence value of each sample, and F_c is the fluorescence of the control.

Results and discussion

Characterization of AgNPs obtained with two types of quercetin

After adding the quercetin solution to the silver nitrate solution, the formation of AgNPs was first evaluated by observing a color change for R1 from orange to brown and for S2 from yellow to brown-reddish, as observed in the inset of Fig. 1a. To fully confirm the obtaining of AgNPs by using both types of quercetins, UV–Vis spectra were recorded at 2 and 24 h. In Fig. 1, it was possible to observe peaks at around 420 nm, which is the characteristic peak of AgNPs that confirm the formation and stability of silver nanoparticles in both aqueous colloidal solutions. The effect of each quercetin was observed in the intensity and value of the absorption band; as can be seen on increasing the purity of quercetin, a redshift in the absorption band to a longer wavelength (from 415 to 450 nm for dietary supplement and reactive grade, respectively) was observed. While in the spectra at 24 h, it is possible to examine that the band intensity increased, indicating a higher presence of AgNPs. The same behavior as previously was observed; higher purity of quercetin (R1) caused absorption to greater wavelength. It is well known that a higher wavelength indicates an increase in the size of synthesized AgNPs. Therefore, the nanoparticles prepared from R1 (reactive grade) are expected to be bigger than S2 (dietary supplement).

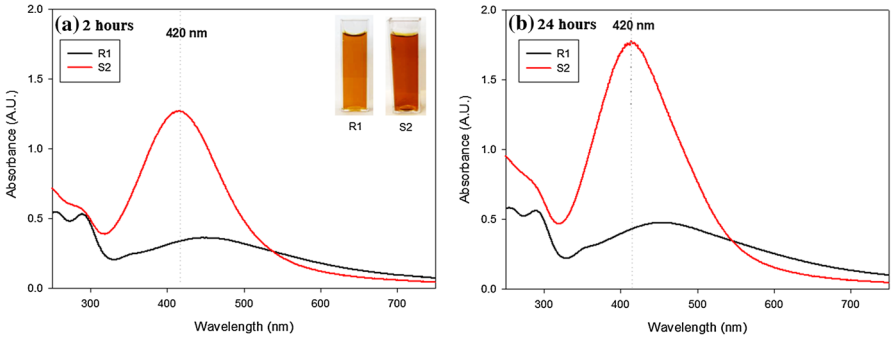

Fig. 1 UV/Vis spectra of AgNPs for each type of quercetin at **a** 2 and **b** 24 h

The morphology and size of the AgNPs were studied by transmission electron microscopy (TEM), and the results are presented in Fig. 2 for the particles synthesized with R1 and S2. Both nanoparticles are nearly spherical and have a relatively uniform size distribution. The micrographs were used to calculate the mean size of the AgNPs, and the results were plotted in a particle size distribution histogram. The size of the AgNPs is smaller when they were obtained from quercetin dietary supplement (S2), since the mean diameter was 6.6 ± 1.9 nm, while for R1 was 8.0 ± 1.7 nm. Besides nanoparticles, agglomerates were also found but were discarded in the previous calculations; nevertheless, they were measured and analyzed to know the size of these clusters. As can be seen in the insets of Fig. 2, the results showed that the AgNPs of R1 tend to form larger agglomerates, in a range of 30 to 85 nm with a mean value of 52.7 ± 10.5 nm, while the AgNPs of S2 tend to form smaller clumps of 20 to 50 nm and a mean value of 29.4 ± 9.6 nm. The size and morphology are indicators that they can function as an antimicrobial material. However, since they are so small (< 10 nm), it is reported that their cytotoxic effect is greater [44]. Therefore, the deposition of these AgNPs on $sTiO_2$ is an excellent option to be safe for use.

Evaluation of cell viability for AgNPs

It is well reported that AgNPs can be classified as hazardous materials due to their cytotoxicity against mammalian cells. Because of this concern, despite being an excellent option as a powerful antibacterial agent, its application is minimal. That is why cell viability studies are carried out to know to what extent and how the use

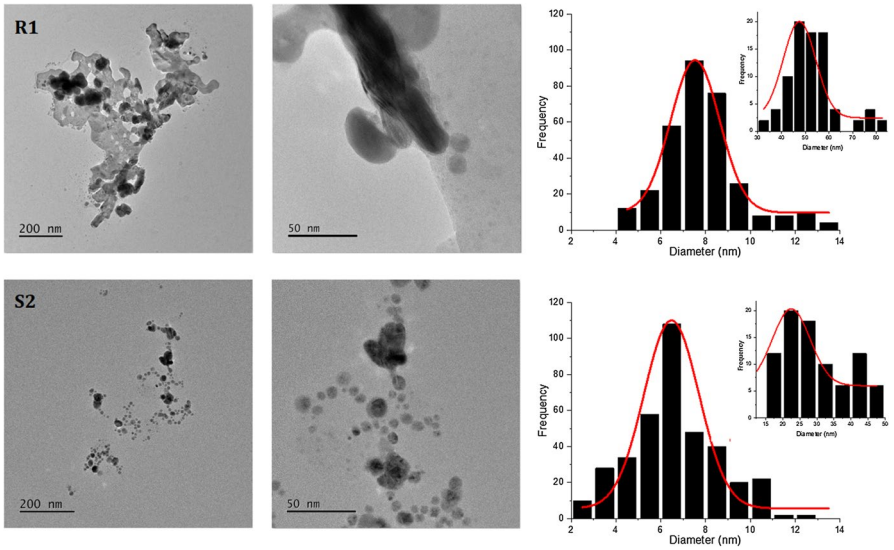

Fig. 2 TEM micrographs and particle size distribution histogram of AgNPs synthesized by each type of quercetin

of these nanoparticles is possible. The cytotoxic effect of the AgNPs and the deposited nanoparticles was evaluated on PBMBC at different concentrations through the Resazurin assay using Eq. 1 [45] in supplemented RPMI-1640 medium (50 U/ml penicillin and 50 mg/ml streptomycin) for 24 h. First, in Fig. 3, the cell viability of AgNPs is reported. Then, as observed for both solutions, R1 and S2, a low% of mitochondrial activity was presented, indicating the synthesized AgNPs present cytotoxicity (at 5 and 10 mL) for this "in vitro" assay. This criterion is reported by ISO 10993–5, which establishes that cell viability must be greater than 80%. Previous studies have found evidence that the cytotoxicity of AgNPs is influenced by a combined effect of the nanometer size and the gross chemical composition of the silver [44, 46]. Therefore, non-cytotoxic activity is expected from Ag deposited on the $sTiO_2$ surface prepared by both methods and from iPP nanocomposites prepared with these nanoparticles.

Characterization of silanized titanium dioxide with APTES

The surface modification of titanium dioxide nanoparticles with APTES was confirmed by Fourier transform infrared spectrometer, which provides information about the functional groups present in the sample. Figure 4 shows the results of the FTIR spectra for pristine TiO_2 (red line) and silanized $sTiO_2$ (black line). As can be seen, new bands appeared after the silanization. The peak at around 1641 cm^{-1} is attributed to the stretching vibration of the (NH)C = O group [47], while the peak at 1566 cm^{-1} corresponds to the flexion of the amino-functional group ($-NH_2$) [8, 47]. The signal at around 1481 cm^{-1} indicates the elastic band of the C-H organic group bond [23, 48]. The peak observed at 1380 cm^{-1} was assigned to the C-N aromatic amine group [49], and the signal observed at 1328 cm^{-1} corresponds to the carbonyl group [50]. In contrast, the peaks at around 1195 and 1040 cm^{-1} are attributed to the Ti–O-C bonds [23, 48, 50]. Finally, the peak at 1037 cm^{-1} can be attributed to the asymmetric extension of the Si–O-Si bond [23, 47, 50]. With all this information, it is possible to confirm that the APTES is bound to the surface of titanium dioxide.

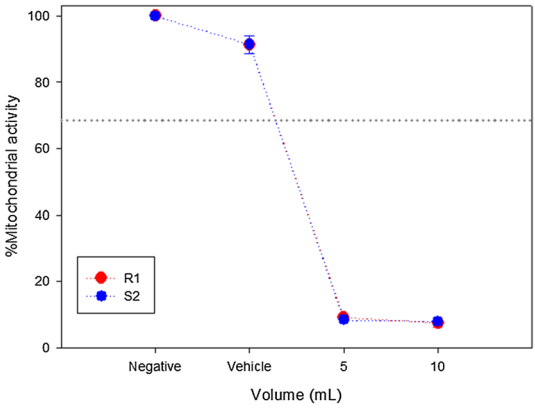

Fig. 3 Cell viability for the AgNPs by the resazurin method

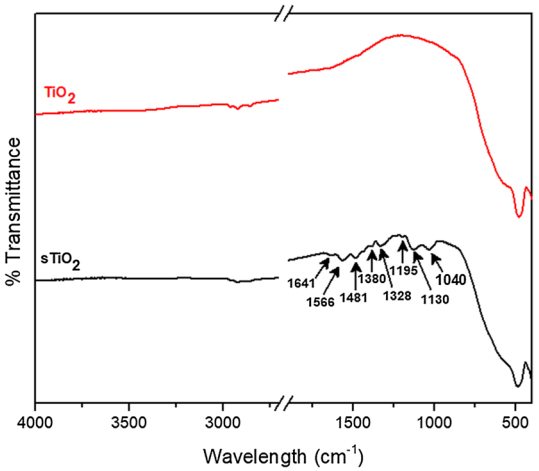

Fig. 4 FTIR spectra for pure TiO_2 and silanized $sTiO_2$

The surface modification of the titanium dioxide with APTES helps enhance dispersion and colloidal stability in the medium by increasing the interaction between the oxide and the AgNPs in an aqueous medium. To confirm the success of silanization, Z-potential profiles as a function of pH and colloidal dispersion were measured for pristine TiO_2 and silanized $sTiO_2$; the results are presented in Fig. 5. As shown in the Z potential outcomes (Fig. 5a), the charge on the surface changed for the silanized system ($sTiO_2$). It is well noted that in an alkaline medium (pH 8 to 11), the absolute values are greater than 30, indicating good colloidal stability in aqueous solutions due to high repulsion among the nanoparticles now due to the amine groups dangling on the surface. This information makes it possible to affirm that silanized nanoparticles present better conditions to avoid instability and agglomeration [51]. In addition, it is possible to observe that the value of the isoelectric point (Z potential equals to zero) was displaced to a higher value, from pH 3.5 for pristine TiO_2 to pH 5.1 for $sTiO_2$, which can be attributed to the influence of the APTES coupling agent due to the alkaline characteristics of the amine groups bonded to the hydroxyl groups on the surface of titanium dioxide promoting repulsion among the particles [7, 52].

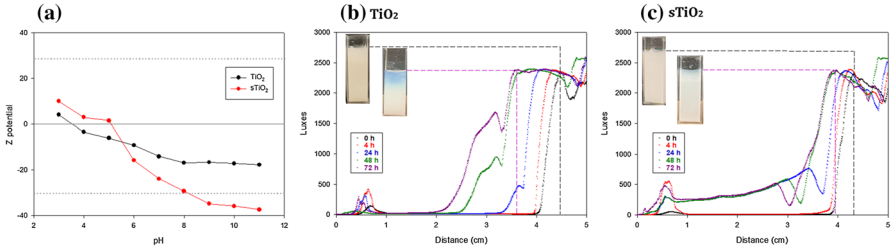

Fig. 5 **a** Z potential for pure TiO_2 and silanized $sTiO_2$, **b** colloidal stability for pure TiO_2, and **c** colloidal stability for silanized $sTiO_2$

However, the results at 0, 4, 24, 48, and 72 h of the colloidal stability test are shown in Fig. 5b and c for pristine TiO_2 and $sTiO_2$, respectively. First, at time 0, the initial state of each system is shown in black dotted lines, and a black dashed line indicates the beginning of the meniscus. At this point, the lux values begin to decrease to a minimum point (0 lx), indicating that the nanoparticles are well-suspended. Then, over time, the values of the suspensions shift to the left (red, blue, green, and purple dotted lines), and different behaviors occur in both systems; for example, in the case of pristine TiO_2 (Fig. 5b), at 24 h there is a substantial change in the measurements with a value of 500 lx, while at 48 and 72 h high values of 1000 and 1700 lx, respectively, are obtained. This behavior indicates that the particles are sedimented, indicating a poor dispersion in water, which can be clearly seen in the inset of Fig. 5b.

On the other hand, the silanized system in Fig. 5c presents better colloidal stability. Unlike the previous system, the lux values are lower for 24, 48, and 72 h, indicating that the system maintained good dispersion. Furthermore, unlike the pristine TiO_2 system, the $sTiO_2$ system showed lux values different from zero (approx. 300 lx), indicating that the particles allow the passage of light, confirming the excellent dispersion of these silanized particles [53], which is in agreement with the results obtained by Z potential regarding the repulsion among particles. The information of both tests confirms the functionalization of the titanium dioxide nanoparticles through the chemical linking of APTES on the oxide surface, which changed its behavior regarding dispersion considerably. Previous works have shown that silanized nanoparticles improve the deposition of AgNPs since the nanoparticles are well-dispersed in the aqueous medium. Therefore, they will interact better and more AgNPs will be deposited on the surface [7, 8].

The formation of AgNPs and their subsequent deposition on the $sTiO_2$ nanoparticles were tested by two methods: the first one (M1) in separate stages to first lead to the reduction of silver ions provided by the dissociation of $AgNO_3$ in water and by the presence of a natural reducing agent like quercetin flavonoid. As a result, the reduction and formation of stable AgNPs at the nanoscale were confirmed by color and UV analysis. The second stage consisted of joining the already formed AgNPs with a colloidal solution of $sTiO_2$ particles so that they interact, and the AgNPs manage to be deposited on the surface of the titania by attractive forces.

While the one-step method (M2) consisted of carrying out the formation and deposition "in situ" at the same time, with the premise that the reducing agent, quercetin, used will provide the dispersion and stability necessary for the reduction of silver ions and the correct interaction to deposit stable nanoscale silver. After performing either method, the deposition, morphology, element content, crystal structure, and behavior of the samples were studied using characterization techniques such as TEM, EDX, XRD, and Z-potential to evaluate which method provides the best conditions to have more Ag deposited on the $sTiO_2$ nanoparticles.

TEM analysis of Ag deposited on $sTiO_2$ nanoparticles

TEM was used to evaluate the Ag deposition on the $sTiO_2$ surface through the two methods and the two types of quercetins. The corresponding images are presented in Fig. 6. This technique is a more or less surface-related analytical tool; this means

that it is possible to obtain an approximate concentration of the analyzed surface. It can be observed that the $sTiO_2$ nanoparticles present AgNPs on the surface and that there is a difference in the amount of Ag that is superficially distributed on the nanoparticle. This difference can be attributed to the method of deposition and the reducing agent used. For example, the systems that use quercetin dietary supplement as a reducing agent of Ag^+ ions presented more silver on the surface. While a remarkable difference is observed when the one-step method (M2) was used for deposition, a large amount of silver is on the surface of the oxide.

Elemental analysis was performed by energy-dispersive X-ray spectroscopy (EDX) to quantify the amount of Ag deposited. The results of all systems for each element are listed in Table 1. Although, as can be seen, the values are according to the TEM images, the less silver content was deposited for the systems prepared with the two-step method (M1), obtaining only 0.8% and 2.7% for M1R1 (quercetin reactive grade) and M1S2 (quercetin dietary supplement), respectively. While for the systems prepared with the one-step method (M2), a greater amount was deposited, 5.0% for M2R1 and 7.0% for M2S2. Nevertheless, the most crucial parameter that enhances the deposition is the type of quercetin; when the dietary supplement was used, the presence of silver increased by 30.6% for the two-step method (M1) and 29.6% for the one-step (M2). Therefore, according to these results, the best system was M2S2 with 7.0% silver content, prepared by the M2 using the dietary supplement as a reducing agent.

X-ray diffraction patterns were used to know the crystalline structure of the $sTiO_2$ particles deposited with Ag. Figure 7 shows the XRD patterns of the four studied systems. It can be observed that the characteristic diffraction at around $2\theta = 27°$, 36°, 39°, 54°, 56°, 62°, 65°, and 69° is related to the (110), (101), (200), (211), (220), (002), (310), and (112) reticular planes of rutile [54]. While the Ag nanoparticle peaks are located at around $2\theta = 38°$, 44°, 64° and 78° assigned to the planes,

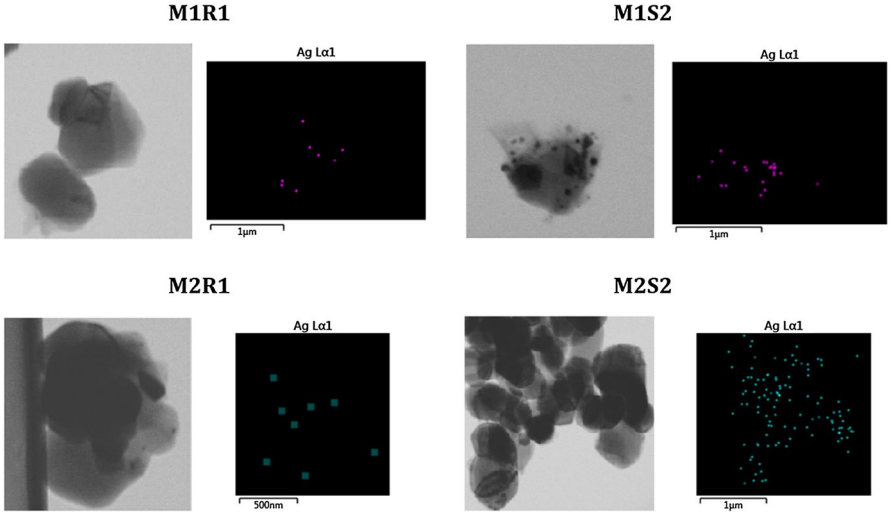

Fig. 6 TEM images and EDX analysis for the four Ag deposited on $sTiO_2$ nanoparticles

Table 1 Weight % of elements in the Ag deposited on $sTiO_2$ nanoparticles obtained from EDX

Element	System			
	Two-step method		One-step method	
	Reagent-grade as reducing agent	Dietary supplement as reducing agent	Reagent-grade as reducing agent	Dietary supplement as reducing agent
	M1R1 (%)	M1S2 (%)	M2R1 (%)	M2R1 (%)
Ti	68.50	52.60	56.40	62.00
O	29.80	31.30	33.00	25.10
Si	0.90	13.30	5.40	5.90
Ag	0.80	2.70	5.20	7.00

(111), (200), (202) and (311), respectively, confirm the crystallinity of the metallic silver in face-cubic-centered (FCC) structure [37]. According to the results, it is possible to validate the results obtained by TEM; the M2S2 system presented the greatest intensity in the peaks corresponding to the AgNPs.

DLS and Zeta potential analysis of Ag deposited on $sTiO_2$ nanoparticles

The comparison of the hydrodynamic diameter of the $sTiO_2$-Ag nanosystems with the nanoparticles before the deposition processes would provide information on the size of the silver particles absorbed on the titania surface [55]. First, the pure and silanized particles were measured by DLS, giving a diameter of 446 nm for pristine TiO_2 and 802.7 nm for $sTiO_2$. This information shows that the hydrodynamic diameter grew considerably due to the long chains of APTES, which was previously confirmed by FTIR and zeta potential in Sect. Characterization of silanized titanium dioxide with APTES. Then, Table 2 shows the average hydrodynamic diameters measured by DLS for the four systems prepared by the two studied methods and

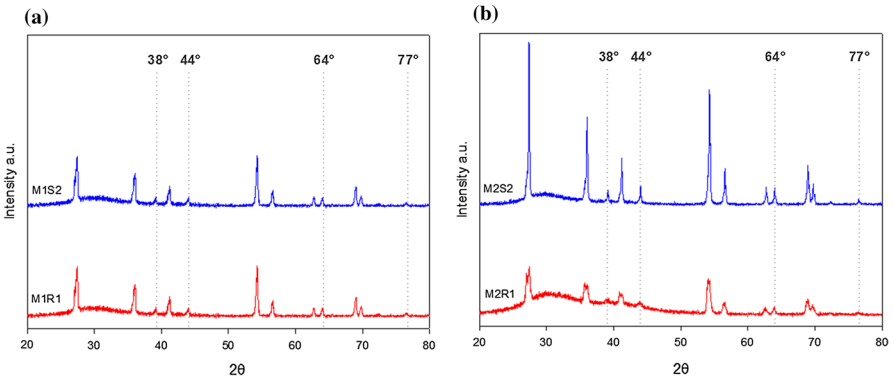

Fig. 7 XRD patterns for the Ag deposited on $sTiO_2$ nanoparticles for **a** two-step method and **b** one-step method

Table 2 Hydrodynamic diameter obtained by DLS of the $sTiO_2$ nanoparticles Ag deposited with AgNPs

Reducing agent	System (Mean value / nm)	
	Two-step method (M1)	One-step method (M2)
Reagent grade	824.9	845.5
Dietary supplement	857.7	898.8

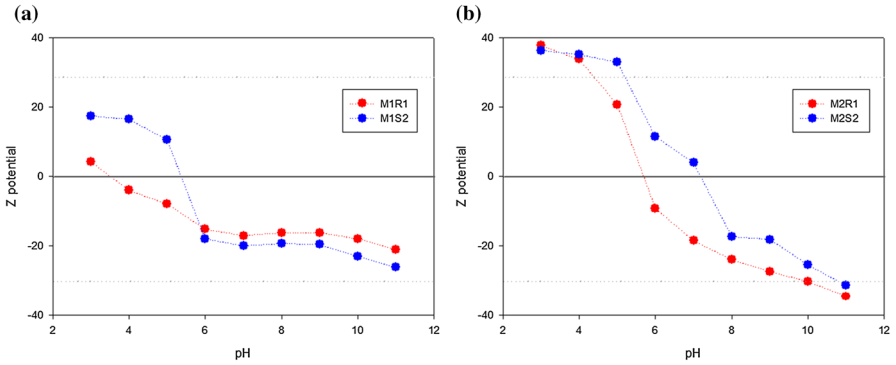

Fig. 8 Z potential results for the Ag deposited on $sTiO_2$ nanoparticles for **a** two-step method and **b** one-step method

using the two types of quercetins. As expected, all the diameters grew up by the presence of Ag deposited on the surface of $sTiO_2$. In addition, the results indicated that the system with the largest diameter was M2S2 (898.8 nm), while the smallest was M1R1 (824.9 nm); this could be explained as that the M2S2 system absorbed around 48 nm of AgNPs on the $sTiO_2$ surface, while the lowest efficiency was the M1R1 system with only approx. 10 nm.

Z potential can be defined as the electrical potential of the nanoparticle interface between the aqueous solution and the stationary layer of ions adhered to the particle [56]. Figure 8 shows that the results of the Z potential tests as a function of pH indicate the surface charge of the four studied systems. As can be seen, the Ag deposited on $sTiO_2$ nanoparticles presents a similar behavior concerning pH; at lower values (acid), they registered positive values, which began to drop down as the pH values increased (alkaline medium). It is well noted that a different isoelectric point (IEP) value was obtained depending on the system. For example, the two-step method (M1) nanoparticles had the lowest values, pH ~ 3.5 for M1R1 and pH ~ 5.3 for M1S2. In contrast, the one-step method (M2) reached higher IEP values, pH ~ 5.8 and ~ 7.2 for M2R1 and M2S2, respectively. When comparing these results with the obtained for $sTiO_2$ discussed in Sect. TEM analysis of Ag deposited on $sTiO_2$ nanoparticles, it is possible to observe that the M1R1 presented a similar behavior to the $sTiO_2$ because this system had the lowest deposition of AgNPs, according to the EDX analysis (Table 1). Therefore, as the presence of AgNPs increased, the values

were proportionally higher due to indicating more presence of positively charged groups on the surface of the titania, since it can be inferred that the surface of the particles, both $sTiO_2$ and AgNPs, is rich in amino groups [57, 58].

Antimicrobial activity of Ag deposited on $sTiO_2$ nanoparticles by disk diffusion method

The antimicrobial activity of the four systems was assessed on two bacteria, *E. coli,* and *S. aureus*, under the disk diffusion method, which is excellent for determining the susceptibility of bacteria to bactericidal agents since it is based on the presence or the absence of a zone of inhibition [59, 60]. The size values of the inhibition zones are shown in Table 3, revealing that depending on the deposition method and the reducing agent used, a different antimicrobial effect was found. Better results were obtained for $sTiO_2$ nanoparticles deposited with the one-step method (M2). Furthermore, while comparing the reducing agent, the dietary supplement showed better efficiency than the reactive grade, up to 40% more. These results were expected since the previous analysis showed that these systems had more silver content (Table 1). On the other hand, a more significant inhibition zone (max. 12.2 mm) was obtained for *S. aureus*. These bacteria have a single-layered and smooth cell wall, making them more susceptible to antibacterial agents. In contrast, *E. coli* had a lower inhibition zone, max. 10.7 mm. This phenomenon may be attributed to Gram-negative bacteria having a double-layered, corrugated cell wall, which gives them greater resistance [36, 61].

The effect of the deposition method is noted; the one-step method (M2) presented more silver on the $sTiO_2$ surface, and the dietary supplement is a more efficient reducing agent for the deposition process. Firstly, this result can be explained by the fact that although the $sTiO_2$ nanoparticles are well-dispersed thanks to the amino groups on the surface, the AgNPs may aggregate, limiting interaction and deposition. Second, our previous work [41] has found that the quercetin dietary supplement has better solubility than reagent-grade quercetin because, although the supplement is only 20% pure, its formulation contains microcrystalline cellulose, an emulsifying and anti-caking agent. Therefore, all these conditions provide a better dispersion of

Table 3 Antibacterial activity by disk diffusion method of the $sTiO_2$ nanoparticles Ag deposited with AgNPs

Bacteria	System (Mean inhibition zone/mm)			
	Two-step method		One-step method	
	Reagent grade as reducing agent	Dietary supplement as reducing agent	Reagent grade as reducing agent	Dietary supplement as reducing agent
	M1R1	M1S2	M2R1	M2S2
S. aureus	8.6	10.0	11.4	12.2
E. coli	8.2	9.4	9.6	10.7

silver and titanium oxide, avoiding aggregation and thus favoring a high surface area and the capture and binding of silver on the $sTiO_2$ nanoparticles [57].

Antibacterial drop-test of the iPP nanocomposites

The iPP nanocomposites prepared at two different ratios of $sTiO_2$ nanoparticles (0.5% w/w and 1% w/w) were tested against two different bacteria following the droplet test described in Sect. Antibacterial analysis of iPP nanocomposites by the drop-test method. As observed in Fig. 9a for *S. aureus* and Fig. 9b for *E. coli*, the results confirmed the antimicrobial activity of $sTiO_2$ nanoparticles deposited on iPP/Ag. As observed, the inhibitory effect of iPP nanocomposites was higher for *S. aureus* than for *E. coli*. This is because Gram-positive cells contain only one layer as a membrane. In contrast, Gram-negative cells have a thin outer membrane, which confers resistance to hydrophobic compounds. Therefore, the cell wall structure plays a vital role in the susceptibility of bacteria in the presence of AgNPs [22, 55].

As for the influence of Ag deposited on $sTiO_2$ nanoparticles, how the deposition was carried out again had a great effect on the antibacterial activity of the nanocomposites. For example, one-step method (M2), "in situ", has the highest inhibition rate (%) on both bacteria, improving the antibacterial effect by 30–37% for S. aureus and 40–70% for E. coli compared to the two-step method (M1). In addition, nanocomposites prepared with Ag deposited on $sTiO_2$ nanoparticles that used the dietary supplement quercetin as a reducing agent had the highest inhibition effect. M2S2 nanocomposites showed 45.5–59.4% inhibition rates against *S. aureus* and 17.4–13.0% against *E. coli*, an improvement of 50% and 80%, respectively, compared to M1R1 nanocomposite, and an improvement of 20% and 35%, respectively, compared to M2R1. This can be attributed to the higher presence of AgNPs in $sTiO_2$ nanoparticles, as confirmed by the above characterization analyses.

Finally, it is essential to mention that the proportion of Ag deposited on $sTiO_2$ nanoparticles on the iPP matrix greatly influences the inhibition rate. For example, better results were obtained for iPP nanocomposites prepared at 0.5% w/w than at 1% w/w. This behavior can be attributed to a low number of nanoparticles being

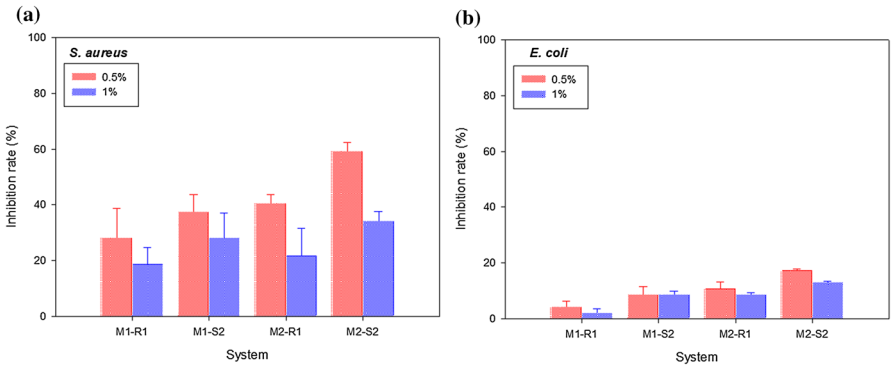

Fig. 9 Inhibition rates for **a** *S. aureus* and **b** *E. coli* by drop-test method

better integrated into the matrix. At the same time, a higher content can cause agglomeration and saturation, counteracting the antibacterial effect of the Ag deposited on the $sTiO_2$ nanoparticles, which according to previous work, is achieved by contact.

Dynamic mechanical analysis of the iPP nanocomposites

DMA is used to evaluate the mechanical properties of polymers; for example, this analysis shows the influence of the Ag deposited on $sTiO_2$ nanoparticles on the physical properties of iPP. This technique consists of applying sinusoidal force to the polymer material deforming the material, providing information about the viscoelastic properties of the polymers [62]. Figure 10 shows the effect of temperature on the storage modulus of the iPP composites prepared at two ratios, 0.5% w/w and 1% w/w. As observed in all graphs, when the temperature increased, the dynamic mechanical behavior of the nanocomposites exhibited less elastic behavior, and the viscous one began to dominate; this change is reflected by the decrease in the values of the storage modulus for all samples.

Figures 10a and b show the storage modulus as a function of temperature for the nanocomposites prepared with Ag deposited on $sTiO_2$ at 0.5% w/w. These results show that at this specific concentration, the storage modulus at 0 °C only increased for the composites prepared with one-step method (M2), the improvement was about

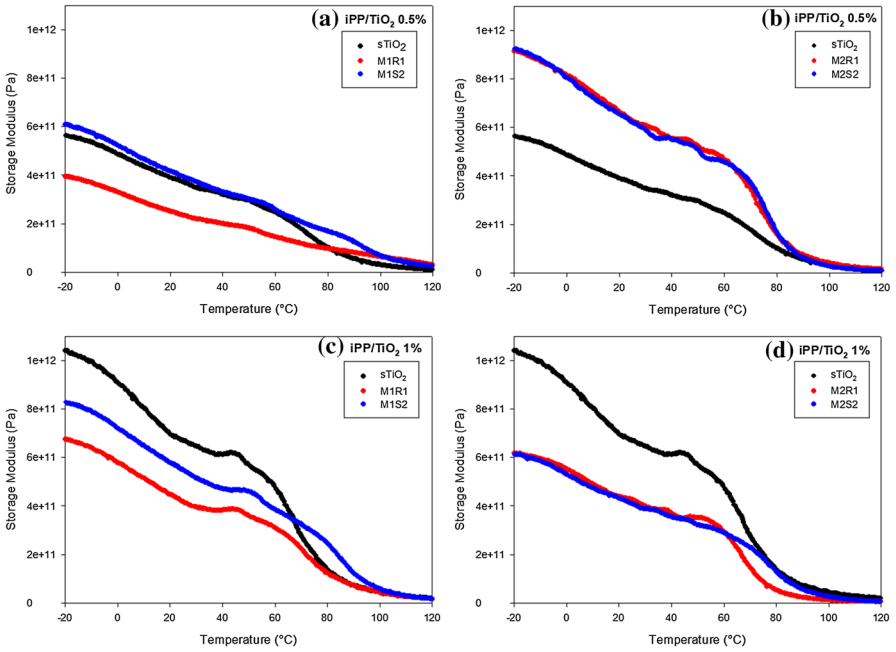

Fig. 10 Storage modulus curves of nanocomposites: **a** iPP/$sTiO_2$ 0.5% by method 1, **b** iPP/$sTiO_2$ 0.5% by method 2, **c** iPP/$sTiO_2$ 1% by method 1, and **d** iPP/$sTiO_2$ 1% by method 2

66% since the nanocomposites prepared with iPP/$sTiO_2$ had values of 5.76×10^{11} Pa, while the iPP nanocomposites with deposited $sTiO_2$ had 9.57×10^{11} Pa for M2R1 and 9.58×10^{11} Pa for M2S2. This increase can be related to the mechanical reinforcement provided by the Ag deposited on $sTiO_2$ nanoparticles into the iPP matrix since this reflects an increase in the rigidity of the nanocomposite. It was clear from Sect. TEM analysis of Ag deposited on $sTiO_2$ nanoparticles, that M2R1 and M2S2 nanocomposites presented the highest content of silver on the $sTiO_2$ surface. This behavior can be attributed to the excellent dispersion of Ag deposited on $sTiO_2$ nanoparticles into the iPP matrix due to the AgNPs presence since The dispersion of the nanoparticles was better, contributing to a better distribution of the applied stress in the matrix [63]. It is essential to mention that higher values were obtained for 0.5% w/w of nanofiller, while the storage modulus decreases for 1% w/w (Fig. 10 c and d). According to previous works, this decrease has been related to cluster formation of the nanoparticles into the polymer matrix. Since increasing the number of nanoparticles in the polymer matrix favors the formation of aggregates, more defective spots will also be produced in the matrix [63, 64].

Figure 11 shows the loss modulus of the nanocomposites, which is associated with the amount of energy that a material can dissipate due to the molecular mobility by the polymer chains [51]. As observed in all images, the loss modulus of all nanocomposites has two significant peaks corresponding to two polymer transitions: the α- and the β-transitions. First, iPP nanocomposites has an α-transition centered at around 68 °C, while the β-transition was found at about 5 °C. The first one is related to the crystalline phase of the polymer, while the second one can be related to the movement in the amorphous region during the glass transition [65]. When a 0.5% w/w ratio was integrated into the polymer, only the nanocomposites with fillers deposited with the one-step method (M2) showed an increase in the loss modulus, having values of 3.42×10^{10} Pa for M2R1 and 3.67×10^{10} Pa for M2S2 at a temperature of 70 °C. This is an improvement of 66% and 72%, when compared to the iPP/$sTiO_2$ (2.06×10^{10} Pa). This means that when more silver was present in the nanocomposite, the integration increased since the energy was better dissipated. According to the results, the nanoparticles deposited with the one-step method (M2R1 and M2S2) at 0.05% w/w are so well dispersed in the nanocomposites that the mechanical properties were significantly improved in integration and stress dissipation, and thus, the antimicrobial capacity enhanced. This behavior can be attributed to the AgNPs that can absorb and dissipate faster the energy near the iPP chains [66]. On the contrary, the loss modulus decreased when the nanocomposites were prepared at 1%; it means that they became flexible, or this ratio is not suitable as reinforcement, probably due to agglomeration [63].

Evaluation of cell viability for Ag deposited on $sTiO_2$ nanoparticles and iPP nanocomposites

Figure 12 shows the results for each $sTiO_2$-Ag system. According to the graphs, there are no significant effects on the reducing agent or method, and the cell viability decreases with the increasing concentration of Ag deposited on $sTiO_2$ nanoparticles.

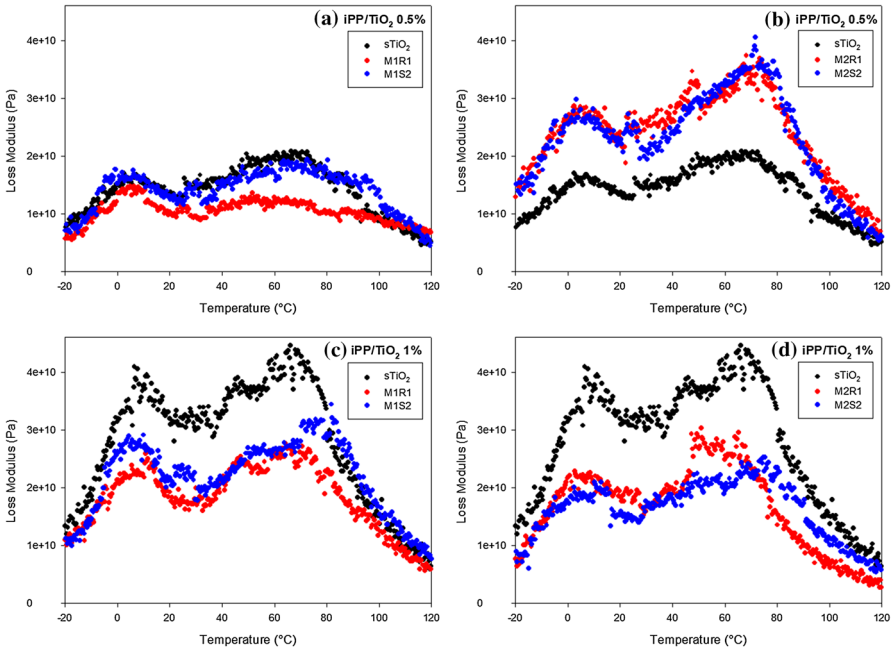

Fig. 11 Loss modulus curves of nanocomposites: **a** iPP/$sTiO_2$ 0.5% by method 1, **b** iPP/$sTiO_2$ 0.5% by method 2, **c** iPP/$sTiO_2$ 1% by method 1, and **d** iPP/$sTiO_2$ 1% by method 2

At low concentrations, no significant cytotoxicity was observed for either system; therefore, it is possible to state that the Ag deposited on $sTiO_2$ does not have adverse effects on the PBMC viability during 24 h of exposure up to 20–50 ppm, implying safe usage at these concentrations [67]. In literature [67–69], it has been reported that the cytotoxic effects of AgNPs could be correlated to their size, shape, and chemical composition. Nevertheless, these resulting Ag deposited on $sTiO_2$ nanoparticles prepared by either method could avoid toxic effects at low concentrations (20–50 ppm) since the cell viability presents values above 80%, which means non-toxic conditions for PBMBC, as stated by the ISO 10993–5:2009, unlike colloidal solutions of AgNPs. This phenomenon can be attributed to two possible reasons: first, the application of green methods for the synthesis of AgNPs and subsequent deposition since the use of hazardous materials such as chemical surfactants, reductants, and solvents was avoided, which could induce cytotoxicity due to their toxic nature [67, 69], and second, the fact that the AgNPs are supported and bonded in a non-toxic material ($sTiO_2$), which avoids the migration of the nanoparticles and reduces the toxicity of AgNPs since they are size-dependent and small particles induce higher cytotoxicity than large ones [70, 71].

In addition, the cell viability of the iPP nanocomposites was also evaluated on PBMBC at three different concentrations (2.2%, 4.4%, and 6.6%) through Resazurin assay. Figure 12 shows the results for each compound prepared at 0.5% and 1% w/w. According to this, it is possible to state that the resulting solutions do not negatively affect the viability of PBMCs compared to the control sample, although AgNPs

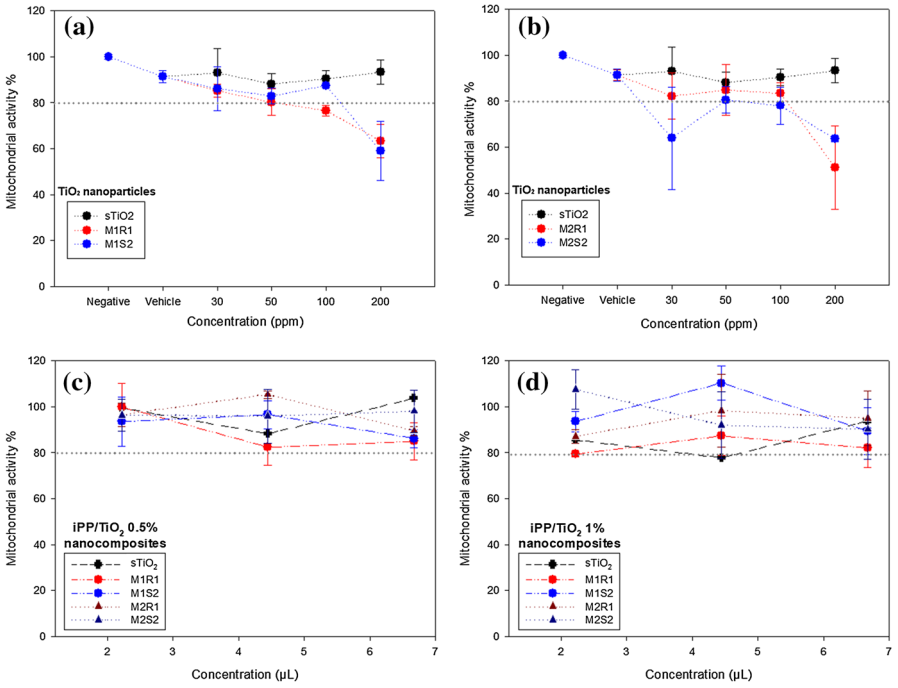

Fig. 12 Cell viability for the Ag deposited on TiO_2 nanoparticles for **a** two-step method and **b** one-step method and for the nanocomposites, **c** iPP/$sTiO_2$ 0.5% and **d** iPP/$sTiO_2$ 1%

exhibited cytotoxicity when evaluated alone. The composites did not exert a toxic effect since cell viability was higher than 80%, which represents non-toxic conditions for cells, according to ISO 10993–5:2009.

Conclusions

According to the complete evaluation, it was found that it is possible to confer antimicrobial activity to the iPP nanocomposites by incorporating Ag deposited on $sTiO_2$ as filler. In addition, it was established that depending on the method used to deposit $sTiO_2$ with AgNPs, each type of filler was incorporated differently into the polymeric matrix.

First, it was demonstrated that reducing silver ions and the subsequent deposition of AgNPs on titanium dioxide surface is feasible by two eco-friendly methods and different quality of reducing agent. Furthermore, the resulting deposited nanomaterials and iPP nanocomposites presented promising antibacterial and non-toxicity activity. In addition, the results indicated that dietary supplement quercetin (with only 20% of purity) improves the solubility in the reaction medium, favoring the reduction and deposition of AgNPs, which resulted in more silver content on $sTiO_2$ surface. In addition, it was found that the one step-method (M2) is better than the two-step method (M1) because the first one simplified the

synthesis and prevented the agglomeration of silver in the second step (deposition), thus improving the dispersion of all particles in the reaction medium. The best nanosystem was M2S2, prepared by the one-step method (M2) and with dietary supplement quercetin, which increased its antibacterial activity up to 40% for *S. aureus* and 30% for *E. coli*. Furthermore, it was demonstrated that these Ag deposited on $sTiO_2$ nanoparticles could be considered non-toxic since, at low concentrations (100 ppm), they do not exhibit cytotoxic activity against seeded peripheral blood mononuclear cells (PBMC), unlike colloidal solutions with a small size (< 10 nm). Therefore, this green one-step method (M2) will allow increasing the applicability of the Ag deposited on $sTiO_2$ nanoparticles to control pathogenic infections. According to the favorable results of this work, there is a great perspective to use these nanoparticles with high antimicrobial power and without cytotoxic effects, to be used at industrial and commercial level in medicine, food, as reinforcement in polymeric matrices, coating in textile fibers, water purification, biomolecules, environment, among others.

The above results are fundamental since the inhibitory effect was replicated in the nanocomposites as obtained in the deposited nanoparticles; the best results were for the nanocomposites prepared with fillers modified by the one-step method (M2), "in situ". Regarding mechanical properties, better results were obtained when method 2 nanoparticles were used as fillers, indicating that these nanosystems are better integrated into the polymer matrix, and therefore, their antimicrobial capacity is outstanding. Finally, iPP nanocomposites with these nanoparticles are non-toxic as there is no ion migration from the polymeric matrix, which helps to enhance the prolonged surface antibacterial effect. Therefore, according to the favorable research results, it opens a wide perspective on the use of Ag deposited on $sTiO_2$, previously silanized, to create antimicrobial and non-toxic iPP composites that can be used at industrial and commercial level in the medical, food and agricultural fields, among others.

Acknowledgements The authors acknowledge Joazet Ojeda and Claudia Hernández for their support during the TEM and XRD analyses, respectively.

Author contributions M.G. Peña-Juárez performed formal analysis, methodology, and writing—original draft. L.O. Sanchez-Vargas, E.J. Gutierrez-Castañeda, and J. Navarrete-Damián did formal analysis. L.A. Flores-Gonzalez validated the study. A. Almendárez-Camarillo did formal analysis and review and editing… E. Pérez supervised the study. J.A. González-Calderón was involved in conceptualization, review and editing, writing—original draft.

Funding M.G. Peña-Juárez and J.A. Gonzalez-Calderón wish to thank to Consejo Nacional de Ciencia y Tecnología (Conacyt México) for PhD scholarship (No: 744689) and for the support with the program "Cátedras-Conacyt", respectively.

Data availability All data generated or analyzed during this study are included in this published article.

Declarations

Conflict of interest The authors declare that they have no conflict of interest.

References

1. Bauer AW, WMM MD, Kirby MDJC, Sherris MDA and Turck MMD (1966) Antiobiotic Susceptibility By A Standardized Single Disk Method. 45: 493–496.
2. Alimunnisa J, Ravichandran K, Meena KS (2017) Synthesis and characterization of Ag@SiO2 core-shell nanoparticles for antibacterial and environmental applications. J Mol Liq 231(2017):281–287. https://doi.org/10.1016/j.molliq.2017.01.103
3. Altan M, Yildirim H (2012) Mechanical and antibacterial properties of injection molded polypropylene/TiO2 nano-composites: effects of surface modification. J Mater Sci Technol. 28:686–692. https://doi.org/10.1016/S1005-0302(12)60116-9
4. Anastacio-López ZS, Gonzalez-Calderon JA, Saldivar-Guerrero R, Velasco-Santos C, Martínez-Hernández AL, Fierro-González JC, Almendárez-Camarillo A (2019) Modification of graphene oxide to induce beta crystals in isotactic polypropylene. J Mater Sci. 54:427–443. https://doi.org/10.1007/s10853-018-2866-3
5. Angkaew S, Limsuwan P (2012) Preparation of silver-titanium dioxide core-shell (Ag@TiO2) nanoparticles: Effect of Ti-Ag mole ratio. Procedia Eng 32(2012):649–655. https://doi.org/10.1016/j.proeng.2012.01.1322
6. Aragundy E, Salas V and Torres F (2011) Modificación de la Superficie del Titanio para Mejorar su Biocompatibilidad mediante la Aplicación de Técnicas de Recubrimiento con Aminas.
7. Auffan M, Rose J, Bottero J-Y, Lowry GV, Jolivet J-P, Wiesner MR (2009) Towards a definition of inorganic nanoparticles from an environmental, health and safety perspective. Nat Nanotechnol 4(10):634–641. https://doi.org/10.1038/nnano.2009.242
8. Azouri A, Ge M, Xun K, Sattler K, Lichwa J and Ray C (2006) Zeta potential studies of titanium dioxide and silver nanoparticle composites in water-based colloidal suspension. Proceedings of 2006 Multifunctional Nanocomposites International Conference. DOI:https://doi.org/10.1115/mn2006-17072.
9. Bardania H, Mahmoudi R, Bagheri H, Salehpour Z, Fouani MH, Darabian B, Khoramrooz SS, Mousavizadeh A, Kowsari M, Moosavifard SE, Christiansen G, Javeshghani D, Alipour M, Akrami M (2020) Facile preparation of a novel biogenic silver-loaded Nanofilm with intrinsic anti-bacterial and oxidant scavenging activities for wound healing. Sci Rep. https://doi.org/10.1038/s41598-020-63032-5
10. Busquets i Alibés E (2013) Breve historia de la ética.
11. Črešnar KP, Aulova A, Bikiaris DN, Lambropoulou D, Kuzmi K and Fras L (2021) Incorporation of Metal - Based Nanoadditives into the PLA Matrix : Effect of Surface Properties on Antibacterial Activity and Mechanical Performance of PLA Nanoadditive Films. (2021)
12. Choffnes ER and Institute of Medicine (U.S.). Forum on Microbial Threats. (2012) Improving food safety through a one health approach : workshop summary, p 395.
13. Chowdhury NR, MacGregor-Ramiasa M, Zilm P, Majewski P, Vasilev K (2016) 'Chocolate' silver nanoparticles: synthesis, antibacterial activity and cytotoxicity. J Colloid Interface Sci 482(2016):151–158. https://doi.org/10.1016/j.jcis.2016.08.003
14. Clinical and Laboratory Standards Institute (2012) Performance standards for antimicrobial disk susceptibility tests: Approved standard - Eleventh edition.
15. Cristea Mariana, Ionita Daniela, Iftime Manuela Maria (2020) Dynamic mechanical analysis investigations of pla-based renewable materials: How are they useful? Materials 13(22):5302. https://doi.org/10.3390/ma13225302
16. Criteria NRC (1985) (US) S. on M. An evaluation of the role of microbiological criteria for foods and food ingredients. An Evaluat Role Microbiolo Criteria Foods Food Ingredients. https://doi.org/10.17226/372
17. Dai X, Zhang Z, Wang C, Ding Q, Jiang J, Mai K (2013) A novel montmorillonite with β-nucleating surface for enhancing β-crystallization of isotactic polypropylene. Compos Part A: Appl Sci Manufact 49:1–8. https://doi.org/10.1016/j.compositesa.2013.01.016
18. Decraemer W, Hunt DJ (2006) Structure and classification. Plant Nematology. https://doi.org/10.1079/9781845930561.0003
19. Alvarado ED, PeñaJuárez MG, Perez CP, Perez E, Gonzalez JA (2019) Improvement in the dispersion of TiO2 particles inside Chitosan-Methyl cellulose films by the use of silane coupling agent. J Mexican Chem Soc. https://doi.org/10.29356/jmcs.v63i2.741

20. Dhanalekshmi KI, Meena KS (2014) Comparison of antibacterial activities of Ag@TiO2 and Ag@SiO2 core-shell nanoparticles. Spectrochimica Acta - Part A: Molecular Biomolecular Spectroscopy 128(2014):887–890. https://doi.org/10.1016/j.saa.2014.02.063
21. Doron S, Gorbach SL (2008) Bacterial infections: overview. Inter Encyclopedia of Public Health 2008:273. https://doi.org/10.1016/B978-012373960-5.00596-7
22. Du J, Sun H (2014) (2014) Polymer/TiO2 hybrid vesicles for excellent UV screening and effective encapsulation of antioxidant agents. ACS Appl Mater Inter 6:13535–13541. https://doi.org/10.1021/am502663j
23. Evans AS and Brachman PS (1998) Bacterial Infections of Humans : Epidemiology and Control., 888.
24. Gallegos-Medrano KK, Escobar-Barrios V, Santamaría-Razo DA, Gutierrez-Castañeda EJ, Vallejo Montesinos J, Peña-Juarez MG, Gonzalez-Calderon JA (2021) Influence of chain length, particle size, and thermal treatment of dicarboxylic acid-functionalized titanium dioxide filler in polypropylene. J Mater Res 36(8):1718–1729. https://doi.org/10.1557/s43578-021-00168-8
25. Hajipour MJ, Fromm KM, Ashkarran AA, Jimenez D, de Aberasturi I, de Larramendi R, Rojo T, Serpooshan V, Parak WJ, Mahmoudi M (2012) Antibacterial properties of nanoparticles. Trends in Biotechnol 30(10):499–511. https://doi.org/10.1016/j.tibtech.2012.06.004
26. Han JW, Gurunathan S, Jeong J-K, Choi Y-J, Kwon D-N, Park J-K, Kim J-H (2014) Oxidative stress mediated cytotoxicity of biologically synthesized silver nanoparticles in human lung epithelial adenocarcinoma cell line. Nanoscale Res Lett. https://doi.org/10.1186/1556-276X-9-459
27. Harikishore M, Sandhyarani M, Venkateswarlu K, Nellaippan TA, Rameshbabu N (2014) Effect of Ag doping on antibacterial and photocatalytic Activity of nanocrystalline TiO2. Procedia Mater Sci 6:557–566. https://doi.org/10.1016/j.mspro.2014.07.071
28. Hoque MIU, Chowdhury AN, Islam MT, Firoz SH, Luba U, Alowasheeir A, Rahman MM, Rehman AU, Ahmad SHA, Holze R, Hossain MSA, Rahman S, Donne SW, Kaneti YV (2021) Fabrication of highly and poorly oxidized silver oxide/silver/tin(IV) oxide nanocomposites and their comparative anti-pathogenic properties towards hazardous food pathogens. Journal of Hazardous Materials. 408:124896
29. Jain S, Mehata MS (2017) Medicinal plant leaf extract and pure flavonoid mediated green synthesis of silver nanoparticles and their enhanced antibacterial property. Sci Rep 7:1–13. https://doi.org/10.1038/s41598-017-15724-8
30. Jardón-Maximino N, Cadenas-Pliego G, Ávila-Orta CA, Comparán-Padilla VE, Lugo-Uribe LE, Pérez-Alvarez M, Tavizón SF, DejesúsSosaSantillán G (2021) Antimicrobial property of polypropylene composites and functionalized copper nanoparticles. Polymers. https://doi.org/10.3390/polym13111694
31. Jastrzębska AM, Kurtycz P, Olszyna A, Karwowska E, Miaśkiewicz-Pęska E, Załęska-Radziwiłł M, Doskocz N, Basiak D (2015) The impact of zeta potential and physicochemical properties of TiO2-based nanocomposites on their biological activity. Inter J Appl Ceramic Technol 12(6):1157–1173. https://doi.org/10.1111/ijac.12340
32. Jeong Y, Lim DW, Choi J (2014) Assessment of size-dependent antimicrobial and cytotoxic properties of silver nanoparticles. Adv Mater Sci Eng 2014:1–6. https://doi.org/10.1155/2014/763807
33. Jiang X, Chunjiao L, Tang M, Yang Z, Jia W, Ma Y, Jia P, Pei D, Wang H (2018) Nanotoxicity of silver nanoparticles on HEK293T Cells: a combined study using biomechanical and biological techniques. ACS Omega 3(6):6770–6778. https://doi.org/10.1021/acsomega.8b00608
34. Sultan Karagoz N, Kiremitler B, Sakir M, Samaa Salem M, Onses S, Sahmetlioglu E, Ceylan A, Yilmaz E (2020) Synthesis of Ag and TiO2 modified polycaprolactone electrospun nanofibers (PCL/TiO2-Ag NFs) as a multifunctional material for SERS, photocatalysis and antibacterial applications. Ecotoxicol Environ Safety 188:109856. https://doi.org/10.1016/j.ecoenv.2019.109856
35. Kawata K, Osawa M, Okabe S (2009) In vitro toxicity of silver nanoparticles at noncytotoxic doses to HepG2 human hepatoma cells. Environ Sci Technol. 43(15):6046–6051. https://doi.org/10.1021/es900754q
36. Keith Nelson, J. (2007) Overview of nanodielectrics: Insulating materials of the future. 2007 Electrical Insulation Conference and Electrical Manufacturing Expo. pp 229–235.
37. León A, Reuquen P, Garín C, Segura R, Vargas P, Zapata P, Orihuela PA (2017) FTIR and raman characterization of TiO2 nanoparticles coated with polyethylene glycol as carrier for 2-methoxyestradiol. Appl Sci (Switzerland). 7(1):1–9. https://doi.org/10.3390/app7010049

38. Li Y, Ma M, Chen W, Li L, Zen M (2011) Preparation of Ag-doped TiO2 nanoparticles by a miniemulsion method and their photoactivity in visible light illuminations. Mater Chem Phys 129(1–2):501–505. https://doi.org/10.1016/j.matchemphys.2011.04.055
39. Liao C, Li Y, Tjong SC (2019) Bactericidal and cytotoxic properties of silver nanoparticles. Inter J Molecu Sci. 20:2. https://doi.org/10.3390/ijms20020449
40. López-Zamora L, Martínez-Martínez HN, González-Calderón JA (2018) Improvement of the colloidal stability of titanium dioxide particles in water through silicon based coupling agent. Mater Chem Phys 217(2018):285–290. https://doi.org/10.1016/j.matchemphys.2018.06.063
41. López-Zamora L, Martínez-Martínez HN, González-Calderón JA (2018) Improvement of the colloidal stability of titanium dioxide particles in water through silicon based coupling agent. Mater Chem Phys 217:285–290. https://doi.org/10.1016/j.matchemphys.2018.06.063
42. Maier C, and Calafut T (1998) Polypropylene : the definitive user's guide and databook. Plastics Design Library.
43. Maye Bernal R, Miguel Guzman U (1984) Antibiograma E Discos Normallzaclon De La Tecnica De Kirby-Bauer. Biomedica. https://doi.org/10.7705/biomedica.v4i3-4.1891
44. Mbenga Y, Mthiyane MN, Botha TL, Horn S, Pieters R, Wepener V, Onwudiwe DC (2022) Nanoarchitectonics of ZnO nanoparticles mediated by extract of tulbaghia violacea and their cytotoxicity evaluation. J Inorganic Organometall Polymers Materals. https://doi.org/10.1007/s10904-022-02248-6
45. Mendoza G, Peña-Juárez MG, Perez E, Gonzalez-Calderon JA (2020) Used of chemically modified titanium dioxide particles to mediate the non-isothermal cold crystallization of poly(latic acid). J Mexican Chem Soc. 64(2):44–63. https://doi.org/10.29356/jmcs.v64i2.1126
46. Molaba MP, Dudić D, Luyt AS (2015) Influence of the presence of medium-soft paraffin wax on the morphology and properties of iPP/silver nanocomposites. Express Polymer Letters 9(10):901–915. https://doi.org/10.3144/expresspolymlett.2015.82
47. Molefi JA, Luyt AS, Krupa I (2010) Comparison of the influence of copper micro- and nano-particles on the mechanical properties of polyethylene/copper composites. J Mater Sci. 45(1):82–88. https://doi.org/10.1007/s10853-009-3894-9
48. Montes-Zavala I, Castrejón-González EO, Rico-Ramírez V, Pérez E, Santamaría-Razo DA, González-Calderón JA (2020) Which is better ? Experimental and simulation analyses of the chemical modification of carbon nanotubes to improve their dispersion in water. J Dispersion Sci Technol. https://doi.org/10.1080/01932691.2020.1763179
49. Montes-Zavala I, Pérez-González MJ, Castrejón-González EO, Santamaría-Razo DA, Almendárez-Camarillo A, Pérez E, Gonzalez-Calderon JA (2021) Thermal and mechanical properties of poly(lactic acid) filled with modified silicon dioxide: importance of the surface area. Polymer Bulletin 1(1–27):0123456789. https://doi.org/10.1007/s00289-021-03571-7
50. Mukhopadhyay A, Basak S, Das JK, Medda SK, Chattopadhyay K, De G (2010) Ag-TiO2 nanoparticle codoped SiO2 films on ZrO 2 barrier-coated glass substrates with antibacterial activity in ambient condition. ACS Appl Mater Inter. 2(9):2540–2546. https://doi.org/10.1021/am100363d
51. Natarajan S, Bhuvaneshwari M, Lakshmi DS, Mrudula P, Chandrasekaran N, Mukherjee A (2016) Antibacterial and antifouling activities of chitosan/TiO2/Ag NPs nanocomposite films against packaged drinking water bacterial isolates. Environ Sci Pollut Res. 23(19):19529–19540. https://doi.org/10.1007/s11356-016-7102-6
52. Olivares-Ramírez MA, López-Zamora L, Peña-Juárez MG, Gutiérrez-Castañeda EJ, Gonzalez-Calderon JA (2021) (2021) Application of the response surface methodology for the evaluation of Staphylococcus aureus inhibition. Polymer Bulletin. https://doi.org/10.1007/s00289-021-03822-7
53. Peña-Juarez MG, Mayorga-Colunga PC, Rivera-Hernandez CA, Gutierrez-Castañeda EJ, Navarrete-Damián J, Pérez E, Gonzalez-Calderon JA (2021) Feasibility of quercetin dietary supplement as reducing and stabilizing agent : green route of silver nanoparticles using a bioactive flavonoid. MRS Commun. https://doi.org/10.1557/s43579-021-00063-7
54. Peña-Juárez MG, Robles-Martínez M, Méndez-Rodríguez KB, López-Esparza R, Pérez E, Gonzalez-Calderon JA (2020) Role of the chemical modification of titanium dioxide surface on the interaction with silver nanoparticles and the capability to enhance antimicrobial properties of poly(lactic acid) composites. Polymer Bulletin. https://doi.org/10.1007/s00289-020-03235-y
55. Pleşa I, Noţingher PV, Schlögl S, Sumereder C, Muhr M (2016) Properties of polymer composites used in high-voltage applications. Polymers 8:5. https://doi.org/10.3390/polym8050173

56. Ranjbar-Mohammadi M, Rahimdokht M, Pajootan E (2019) Low cost hydrogels based on gum Tragacanth and TiO2 nanoparticles: characterization and RBFNN modelling of methylene blue dye removal. Int J Biol Macromol 134(2019):967–975. https://doi.org/10.1016/j.ijbiomac.2019.05.026
57. Sabzi M, Mirabedini SM, Zohuriaan-Mehr J, Atai M (2009) Surface modification of TiO2 nanoparticles with silane coupling agent and investigation of its effect on the properties of polyurethane composite coating. Progress in Organic Coatings. 65(2):222–228. https://doi.org/10.1016/j.porgcoat.2008.11.006
58. Saha B, Kumar S, Sengupta S (2019) Green synthesis of nano silver on TiO2 catalyst for application in oxidation of thiophene. Chem Eng Sci. 199:332–341. https://doi.org/10.1016/j.ces.2018.12.063
59. Taylor TA and Unakal CG(2020) Staphylococcus Aureus. Food Microbiology: Fundamentals and Frontiers. pp 555–584.
60. Vallejo-Montesinos J, Gámez-Cordero J, Zarraga R, Pérez Pérez MC, Gonzalez-Calderon JA (2020) Influence of the surface modification of titanium dioxide nanoparticles TiO2 under efficiency of silver nanodots deposition and its effect under the properties of starch–chitosan (SC) films. Polymer Bulletin. 77(1):107–133. https://doi.org/10.1007/s00289-019-02740-z
61. Vallejo W, Díaz-Uribe C, Navarro K, Valle R, Arboleda JW, Romero E (2016) Estudio de la actividad antimicrobiana de películas delgadas de dióxido de titanio modificado con plata. Revista de la Academia Colombiana de Ciencias Exactas, Físicas y Naturales. 40(154):69. https://doi.org/10.18257/raccefyn.289
62. Varga J (2002) β-modification of isotactic polypropylene: preparation, structure, processing, properties and application. J Macromolec Sci, Part B 41(4–6):1121–1171. https://doi.org/10.1081/MB-120013089
63. Wang S-W, Yang W, Bao R-Y, Wang B, Xie B-H, Yang M-B (2010) The enhanced nucleating ability of carbon nanotube-supported β-nucleating agent in isotactic polypropylene. Colloid Polymer Sci. 288(6):681–688. https://doi.org/10.1007/s00396-010-2194-x
64. Wu WY, Hsu CF, Wu MJ, Chen CN, Huang JJ (2017) Ag–TiO2 composite photoelectrode for dye-sensitized solar cell. Appl Phys A: Mater Sci Process 123(5):1–8. https://doi.org/10.1007/s00339-017-0963-9
65. Xing Y, Li X, Zhang L, Xu Q, Che Z, Li W, Bai Y, Li K (2012) Effect of TiO2 nanoparticles on the antibacterial and physical properties of polyethylene-based film. Progress in Organic Coatings 73(2–3):219–224. https://doi.org/10.1016/j.porgcoat.2011.11.005
66. Xue Yuying, Zhang Ting, Zhang Bangyong, Gong Fan, Huang Yanmei, Tang Meng (2016) Cytotoxicity and apoptosis induced by silver nanoparticles in human liver HepG2 cells in different dispersion media: Cytotoxicity and apoptosis of Ag NPs in different dispersion media. Journal of Applied Toxicology 36(3):352–360. https://doi.org/10.1002/jat.3199
67. Yang E-J, Kim S, Kim JS, Choi I-H (2012) Inflammasome formation and IL-1β release by human blood monocytes in response to silver nanoparticles. Biomaterials 33(28):6858–6867. https://doi.org/10.1016/j.biomaterials.2012.06.016
68. Z Han, RG (2008) Overview of polymer nanocomposites as dielectrics and electrical insulation materials for large high voltage rotating machines. Nano Science and Technology Institute.
69. Zhang T, Wang L, Chen Q, Chen C (2014) Cytotoxic potential of silver nanoparticles. Yonsei Medical J. 55(2):283–291. https://doi.org/10.3349/ymj.2014.55.2.283
70. Zhang Y, Fu F, Li Y, Zhang D, Chen Y (2018) One-step synthesis of Ag@TiO2 nanoparticles for enhanced photocatalytic performance. Nanomaterials 8(12):1032. https://doi.org/10.3390/nano8121032
71. Zhang Y, Newton B, Lewis E, Fu PP, Kafoury R, Ray PC, Yu H (2015) Cytotoxicity of organic surface coating agents used for nanoparticles synthesis and stability. Toxicology in Vitro 29(4):762–768. https://doi.org/10.1016/j.tiv.2015.01.017

Publisher's Note Springer Nature remains neutral with regard to jurisdictional claims in published maps and institutional affiliations.